Electric Power Systems Research 212 (2022) 108530

Contents lists available at ScienceDirect

Electric Power Systems Research

journal homepage: www.elsevier.com/locate/epsr

Model-based efficiency and emissions evaluation of a marine hybrid power system with load profile

Pramod Ghimire [a,b], Siamak Karimi [a], Mehdi Zadeh [a,*], Krishna Kumar Nagalingam [c], Eilif Pedersen [a]

[a] Department of Marine Technology, Norwegian University of Science and Technology, Trondhiem, Norway
[b] Maritime Simulation, Kongsberg Digital, Horten, Norway
[c] Hybrid Power System, Kongsberg Maritime, Kongsberg, Norway

ARTICLE INFO

Keywords:
Emissions
Energy efficiency
Marine hybrid power systems
Marine propulsion
Modeling
Onboard DC grid

ABSTRACT

In this paper, an efficiency and emissions evaluation framework for marine DC hybrid power systems is developed based on the physics- and data-based models of the power components. The proposed framework is tested under the operational profile of a real-case semi-submersible drill rig with all-electric propulsion and a suggetsed DC hybrid power system with batteries. The applied load profile, including propulsion, drilling, auxiliary, and hotel loads, shows high fluctuations, indicating the need for battery hybridization. In addition to the operational profile, the impact of the onboard power system configuration, sectionalized and common bus, on the emissions and efficiency has been studied. The results include the total energy efficiency of the ship powertrain from fuel to propulsion load and total CO_2 emissions. For the considered vessel power system and operational profile, it is observed that the sectionalized bus configuration performs slightly better in terms of energy efficiency, and consequently fuel consumption and CO_2 emissions.

1. Introduction

Energy efficiency improvement and emissions reduction have gained significant attention in the maritime industry recently to comply with the stringent regulations put forward by the authorities [1,2]. Thanks to the rapid development of innovative and efficient technologies, the maritime industry has mostly been able to cope with the rules and regulations for both emissions and energy efficiency. Therefore, the maritime industry is complying with already enforced regulations on nitrogen oxides (NO_x) and sulphur oxides (SO_x). However, meeting the high ambitions in greenhouse gas (GHG) emissions reduction imposed by the International Maritime Organization (IMO) remains challenging. It aims to reduce GHG emissions by 50% by 2050 than 2008 and increase the energy efficiency of the new ship builds by at least 30% by 2025 than 2014 [3].

Different tools and measures are used to monitor efficiency and emissions in the ship design and operational phases. The energy efficiency in the new builds is monitored in terms of the energy efficiency design index (EEDI), which is defined as a mass of CO_2 emissions per capacity mile. Additionally, the energy efficiency existing ship index (EEXI), adapted from EEDI, is proposed for the existing and operational vessels, which is calculated based on the CO_2 emissions per cargo ton and mile [4]. The actual operational CO_2 emissions of the vessels are measured using a carbon intensity indicator (CII). Ship energy efficiency management plan (SEEMP) and energy efficiency operational index (EEOI) are the operational measures and monitoring tools for CII, which are applicable for some vessel types from 2023 [5].

To comply with the regulations, various solutions are being investigated and experimented such as alternative fuels, power system advancement, hull optimization, and operational improvements [6]. DC onboard power systems, one of the aforementioned solutions, offer various advantages over conventional AC onboard power systems. For example, DC power systems enable the variable speed operation of engines in the low load regions, improving the energy efficiency [7,8]. Moreover, the DC power system increases flexibility, such as the easier inclusion of energy storage devices such as batteries and supercapacitors [9].

Hybridizing the power system is another promising solution towards efficiency improvement and emissions reduction, thanks to electric propulsion and marine batteries [6,10–12]. However, the planning and operation of batteries should be designed carefully to enhance cost-efficiency in ship operation. In this regard, the dynamic system performance of a marine vessel can be evaluated in terms of energy efficiency, fuel consumption, and emissions. Therefore, it requires reliable

* Corresponding author.
E-mail addresses: pramod.ghimire@ntnu.no (P. Ghimire), mehdi.zadeh@ntnu.no (M. Zadeh).

https://doi.org/10.1016/j.epsr.2022.108530
Received 3 October 2021; Received in revised form 17 April 2022; Accepted 2 July 2022
Available online 26 July 2022

energy efficiency component models and tools to be used in the system and control design along with system performance evaluation [13].

The component efficiency models can vary from the simplified polynomial-based [12] to physics-based analytical models [13]. Further, the efficiency of each component and system as a whole depends on the operating condition, for instance, the output power. Therefore, it is necessary to consider the loading condition. Implementation of an actual load profile from the operating vessel into the simulation framework provides the efficiency evaluation in a realistic scenario such that the results can be reliable. Thus, high-fidelity yet simple physics-based component efficiency models and realistic load profiles are the key factors in the system efficiency evaluation process. However, efficiency and emissions evaluation in a full-scale marine vessel through reliable mechanistic models and operational profile is not well represented in the literature for a marine hybrid power system.

This paper aims to establish a load profile-based efficiency and emissions evaluation tool to evaluate and monitor the efficiency and emissions in operational conditions. The load profile is classified and applied to specific load side components. A battery hybrid system is proposed for a semi-submersible drilling rig as a use case, where one dedicated battery bank is proposed for each bus. The energy efficiency and emissions evaluation are carried out for two simulation cases; one with a common bus and the other with a sectionalized bus. It also investigates the effect of high-level control systems such as the power and energy management system (PEMS) on the battery hybrid system. The rule-based PEMS is used to operate the energy carriers in the hybrid power system in an optimal manner. This work assesses the whole powertrain efficiency using reliable and full-scale component energy efficiency models. For the used vessel power system, operational profile, and the high-level control, it is observed that the sectionalized bus performs slightly better in terms of energy efficiency, fuel consumption, and CO_2 emissions.

The paper is divided into six sections. The studied hybrid power system and the actual load profile of the power system are discussed and analyzed in Section 2 along with efficiency evaluation methodology. Section 3 presents the component loss models and their utilization in the estimation of system energy efficiency and emissions. Section 4 presents the results and discussions on the simulation-based case studies. Finally, the work is concluded in Section 5.

2. Proposed hybrid power system configuration

This work selected the semi-submersible drilling rig as the case study vessel. Such a vessel needs station-keeping capability, especially during the drilling operations. Station keeping in such vessels is performed using a dynamic positioning system along with the diesel–electric power generation and distribution system [14]. The radial or ring is the usual main bus topology in the sem-submersible rigs [14]. Further, a battery hybrid power system with a radial-main bus in a DC system is proposed for the studied vessel, as depicted in Fig. 1.

The vessel power system is divided into three main buses by the bus-tie breakers. The power in each main bus is supplied by two main diesel generators, with the nominal main bus voltage of 1 kV DC. In addition, each bus supplies power to two thrusters and the auxiliary machinery, including drilling and hotel loads. A Li-ion battery bank is incorporated into each as an energy storage device. The primary parameters for the components in each main bus are presented in Table 1, where a total number of each component used in the studied power system is indicated under the Number column.

The semi-submersible drilling rig load is mainly due to the drilling activity and the dynamic positioning. In general, the operational modes in such vessels can be identified as transit, drilling, and back reaming [15]. The dynamic positioning system remains active in all these operating modes. Based on the requirement of position keeping and environmental conditions, the propulsion loads may vary. Therefore, the actual load profile from the operating vessel, as shown in Fig. 2, is used in this study. As implemented load profile represents all three operating modes of a semi-submersible rig, the results and conclusion drawn from this study can be generalized for this specific vessel type.

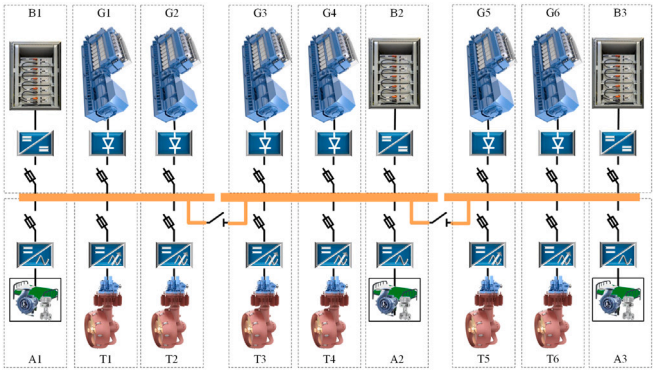

Fig. 1. Power system overview of the studied offshore vessel.

Table 1
Rated parameters and number of components used.

Components	Parameters	Number
Diesel engine	6.1 MW	6
Generator	5.6 MW, 690 V	6
Generator rectifier	5.88 MW	6
Battery	3.36 kAh, 1 kV	3
Battery DC-DC Conv.	3.8 MW	3
Main bus	1 kV DC	1
Thruster inverter	4.2 MW	6
Thruster motor	4.0 MW	6
Auxiliary inverter	7.14 MW	3
Auxiliary load	6.8 MW	3

Based on the main objective of the work, the methodology is developed to improve the performance of the marine hybrid power system with the actual load profiles and physics-based efficiency models, as shown in Fig. 3. The single bus and the interlinked components are used to describe the methodology. The physical component symbols represent their efficiency models. The load profiles measured during the vessel operation are used as the power of propulsion units and auxiliary machinery, including drilling and hotel loads.

The input power can be calculated using loss models for the components for the known output power. Therefore, the terminal variables for the blocks are usually the power input and output. The power system configuration for a drilling rig is established using the developed component efficiency models. The measurement signals, such as bus voltage, and load currents from the main bus, are inputs to the high-level control (PEMS). Based on the power demand and available power, PEMS decides the operation of the generators and battery by providing the power references for battery 1, generator 1, and generator 2 as B1_Pref, G1_Pref, and G2_Pref, respectively. As low-level controls for the components are not modeled, it is assumed that the energy carriers always deliver the requested power.

The amount of fuel required to provide the requested power can be evaluated based on the lower calorific heat value of the fuel and engine efficiency. Using the burned fuel quantity, ship emissions, specially CO_2, can be calculated. Besides, the system model presents the instantaneous (power) and time average (energy) efficiencies. By keeping track of the efficiency and emissions of a vessel, one can develop better high-level control algorithms to improve the system's performance. Further, different operational strategies such as sectionalized and common buses can be tested and utilized to reduce fuel consumption and emissions. Similarly, the developed system model can be used to find a nearly optimal size of battery that can enhance system performance.

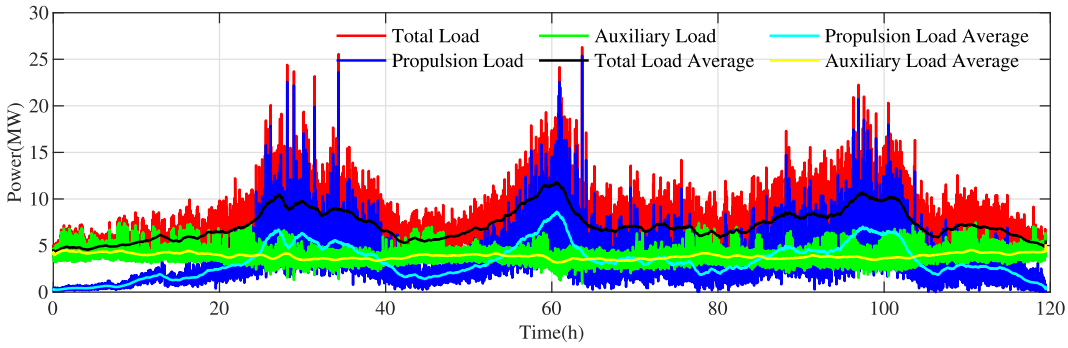

Fig. 2. The total load profile of a drilling rig used in this study.

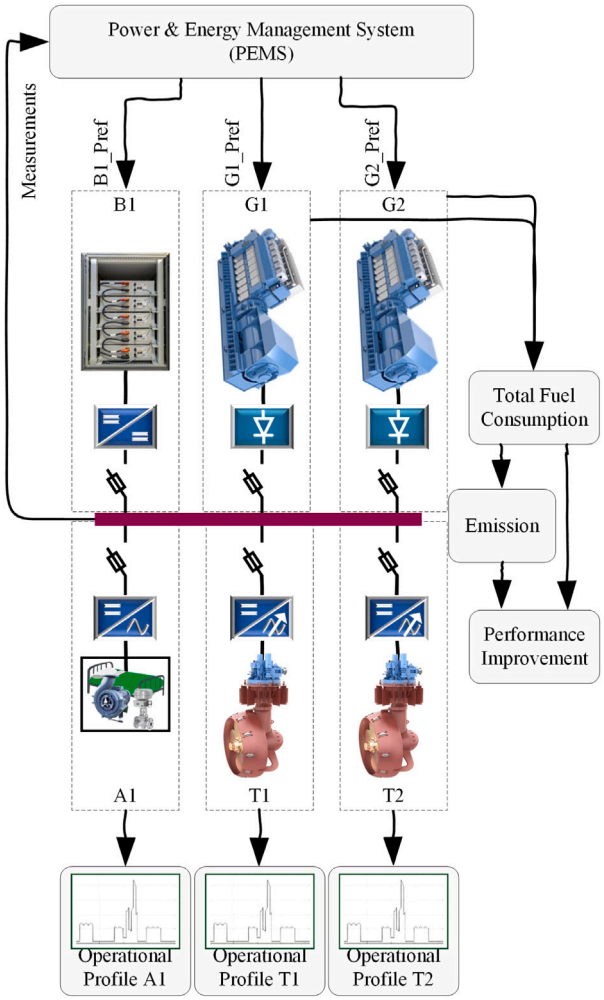

Fig. 3. Efficiency and emissions-based performance improvement methodology.

3. Efficiency modeling

3.1. System efficiency and emissions models

The efficiency of a component (η) is defined as ratio of an output power (P_{out}) to input power (P_{in}). When the power loss (P_{loss}) in the component can be measured or estimated, it can also be used to calculate the component efficiency.

$$\eta = \frac{P_{out}}{P_{in}} = \frac{P_{in} - P_{loss}}{P_{in}} = \frac{P_{out}}{P_{out} + P_{loss}} \tag{1}$$

The actual output and input power in the system are necessary to calculate the system efficiency. However, in the battery hybrid power system, the battery works both as the power consumer and generator. Therefore, battery power is considered input power to the system when it is in discharging mode and output power from the system during charging mode. The power-based efficiency ($\eta_p(t)$) for a hybrid power system is expressed in (2), where P_{Load} is the total load power consisting of propulsion and auxiliary load and P_{Fuel} is the power due to the amount of fuel consumed.

$$\eta_p(t) = \frac{P_{out}(t)}{P_{in}(t)} = \frac{P_{Load}(t) + P_{Batt,ch}(t)}{P_{Fuel}(t) + P_{Batt,disch}(t)} \tag{2}$$

The energy efficiency of the system can then be estimated as a ratio of time integrals of the system input and output power as in (3).

$$\eta_e(t) = \frac{\int P_{out}(t)dt}{\int P_{in}(t)dt} \tag{3}$$

The CO_2 emissions (E_{CO_2}) can be estimated using the total fuel consumed (m_f) and the carbon content (C) in the used fuel [16] as in (4). The carbon content in the marine diesel oil usually varies from 0.862 to 0.867 [17].

$$E_{CO_2} = \frac{44}{12} \cdot C \cdot m_f \tag{4}$$

3.2. 12-pulse diode rectifier

A 12-pulse diode rectifier consists of one three-winding phase shift transformer and two three-phase diode rectifiers, as shown in Fig. 4(a). The power loss components generated in a power transformer are a no-load power loss depending on the voltage (P_{noLoad}) and copper loss dependent on the load (P_{cu}). Thus, by extracting the no-load and copper power loss of a transformer, the transformer power loss may be calculated by the following expression where P_{rated} is rated transformer power and P_{load} is the power drawn through the transformer.

$$P_{Tr,loss} = P_{noLoad} + P_{cu}\left(\frac{P_{load}}{P_{rated}}\right)^2 \tag{5}$$

Regarding the diode rectifier power loss, diodes are modeled as a constant voltage source and a resistance. Further, since the frequency is 50 or 60 Hz turning off power loss is negligible. The following expression calculates the averaged conduction power loss for a diode rectifier where V_{FW0} and r_F are the forward voltage and resistance of the diode, respectively.

$$P_{C,loss} = V_{FW0} I_{FAV} + r_F I_{FRMS}^2 \tag{6}$$

I_{FAV} and I_{FRMS} are the average and root mean square (RMS) of the current passing through a diode. For a 120-degree operation of a diode rectifier, the approximated power loss can be calculated as follows [13].

$$P_{C,loss} = \frac{4}{3}(V_{FW0} I_{out} + r_F I_{out}^2) \tag{7}$$

I_{out} is the averaged output current.

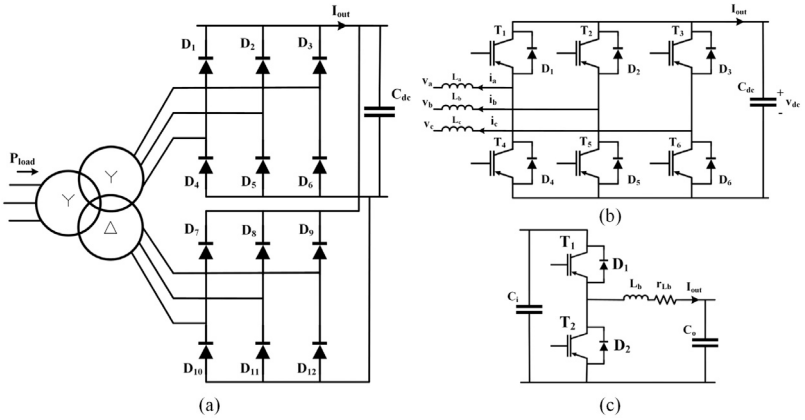

Fig. 4. Power converters. (a) Diode rectifier. (b) Voltage source converter. (c) Buck-boost converter.

3.3. Two-level voltage source converter

Two-level voltage source converters (VSCs) offer a bidirectional DC-AC conversion allowing for power and voltage control. In this work, for interfacing the propulsion motor to the DC bus, three-phase sinusoidal pulse width modulation (SPWM) inverter with six insulated-gate bipolar transistors (IGBTs) and anti-parallel diodes is considered, as shown in Fig. 4(b). Power loss associated with this converter is categorized into a conduction loss and a switching power loss. The conduction loss of an IGBT can be calculated as the following expression [18].

$$P_{C,loss,T} = \left(\frac{1}{2\pi} + \frac{mcos\theta}{8}\right)V_{CE0}I_C + \left(\frac{1}{8} + \frac{mcos\theta}{3\pi}\right)r_{CE}I_C^2 \tag{8}$$

m, I_c, ω, and θ are modulation factor, a peak value of the output current, the frequency of output signal, and the phase shift of the output current and fundamental harmonic of output AC voltage. Moreover, V_{CE0}, r_{CE} are the equivalent voltage and resistance characteristic of the IGBT. For diodes, similar to the calculation of conduction loss for IGBTs, the on-state power dissipation of a diode is calculated by the following expression [18].

$$P_{C,loss,D} = \left(\frac{1}{2\pi} + \frac{mcos\theta}{8}\right)V_{FW0}I_D + \left(\frac{1}{8} - \frac{mcos\theta}{3\pi}\right)r_F I_D^2 \tag{9}$$

Based on the switching loss characteristics of IGBTs provided in their datasheet, turning on and turning off switching losses are linearly and nonlinearly dependent on the collector current and the blocking voltage, respectively. In this regard, the approximated expression for IGBT switching loss is in the following [19].

$$P_{S,loss,T} = \frac{\sqrt{2}f_{sw}(E_{on} + E_{off})}{\pi}\left(\frac{I_{out}}{I_{ref}}\right)\left(\frac{V_{cc}}{V_{ref}}\right)^{1.3} \tag{10}$$

E_{on} and E_{off} are turning on, turning off energy loss with respect to a reference voltage and current, V_{ref} and I_{ref}, in the datasheet. Further, V_{cc} is the blocking voltage over an IGBT. For diodes, only the turning off power loss, E_{rr}, caused by the reverse recovery current, is taken into account [19].

$$P_{S,loss,D} = \frac{\sqrt{2}f_{sw}E_{rr}}{\pi}\left(\frac{I_{out}}{I_{ref}}\right)^{0.6}\left(\frac{V_{cc}}{V_{ref}}\right)^{0.6} \tag{11}$$

3.4. Bidirectional DC-DC converter

In this paper, a buck/boost converter, as shown in Fig. 4(c), is used for the battery energy storage systems. It acts as a buck when the battery is charging and as a boost when discharging. The power loss components are a conduction loss and a switching loss. The averaged conduction loss is calculated by the linear approximation of output characteristics of the IGBT and the diode [20], as shown below in (12)–(14).

$$P_{C,loss,T} = D(V_{CE0}I_{Lb} + r_{CE}I_{Lb}^2) \tag{12}$$

$$P_{C,loss,D} = (1 - D)(V_{FW0}I_{Lb} + r_F I_{Lb}^2) \tag{13}$$

$$P_{R,loss,Lb} = r_{Lb}I_{Lb}^2 \tag{14}$$

r_{Lb} and I_{Lb} are the measured resistance and the current of the boost inductor, respectively. D is the converter's duty cycle, which is the ratio of the battery voltage over DC bus voltage. The switching loss of the transistor and the diode [19] are calculated, as presented in (10) and (11), respectively.

3.5. Li-ion battery

The internal power loss of Li-ion batteries generated in the charging, standby, and discharging stages results in the difference between the energy required for charging a battery from x% SoC to y% SoC and the energy released of discharging it from y% SoC to x% SoC (note that $y > x$). Since the efficiency of a Li-ion battery is dependent on its current, temperature, and SoC, the constant-valued energy efficiency for the battery is not an accurate modeling approach. In this work, the model proposed in [21] for calculation of internal power loss of Li-ion battery energy storage systems based on the voltage drop model [22] is used. In addition, the impact of temperature on power loss is neglected based on the assumption of a perfectly controlled temperature during the operation. The internal power loss generated during the discharging and charging process for Li-ion batteries is shown in the following.

$$P_{B,loss}^D = \frac{q}{vS}\left(r + \frac{k}{SoC}\right)(P^D)^2 + kS\left(\frac{1 - SoC}{SoC}\right)P^D \tag{15}$$

$$P_{B,loss}^C = \frac{q}{vS}\left(r + \frac{k}{1 - SoC}\right)(P^C)^2 + kS\left(\frac{1 - SoC}{SoC}\right)P^C \tag{16}$$

q, v, and r are the maximum ampere-hours, nominal voltage, and internal resistance of a battery cell. Further, S, P^D, and P^C are the energy capacity, discharging, and charging DC power of the battery system. Finally, the parameter k is calculated according to the $1C$ discharge characteristic V–Ah curve of the battery cell as it is described in [21].

3.6. Diesel engine

The specific fuel oil consumption (SFOC) data for implemented variable speed diesel engine W10V31, obtained from Wartsila engine-configurator [23], is used to develop the SFOC and efficiency curve as shown in Fig. 5.

The SFOC curve is represented by a second-order polynomial equation as in (17). At 87% load power, SFOC is minimum, and η is maximum for the considered engine. The SFOC curve can be used to calculate the required fuel flow rate ($\dot{m}_f$, kg/s) to produce engine output power (P_e, W) as in (18). The total fuel consumption (m_f, kg) can then be estimated by integrating the fuel flow rate over the time as

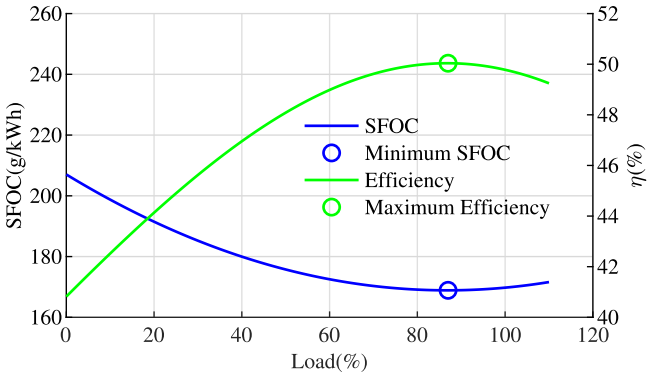

Fig. 5. Typical SFOC and efficiency curves for a diesel engine.

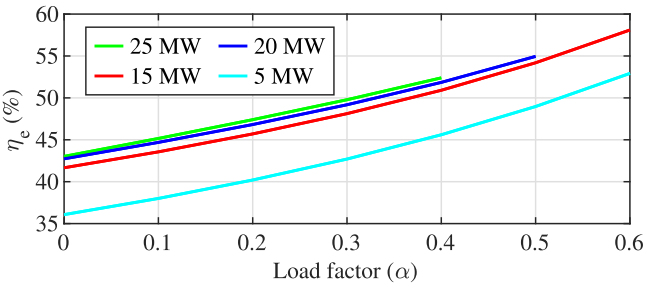

Fig. 6. The energy efficiency variation against time for the fixed load and variable load sharing.

in (19). Further, efficiency of the engine can be evaluated using SFOC and lower calorific heat value h_n as in (20).

$$SFOC = 0.0051x^2 - 0.8787x + 207.0270 \tag{17}$$

$$\dot{m}_f = SFOC \cdot P_e \tag{18}$$

$$m_f = \int \dot{m}_f \cdot dt \tag{19}$$

$$\eta = \frac{1}{SFOC \cdot h_n} \tag{20}$$

4. Results and discussions

The developed models are used for the efficiency and emissions analysis. At the component level, the power converters are assumed to be constructed by identical power electronics switches such as IGBT modules FF1500R17IP5P [24] and diodes VS-SD3000C [25]. For the system-level analysis, two separate case studies are developed based on two diffreent load scenarios such as a fixed power load and a real-case load profile.

4.1. Efficiency analysis for fixed-power loads

In the fisrt case, the power output of the thrusters and auxiliary loads are kept constant at 25 MW, 20 MW, 15 MW and 5 MW, respectively to investigate the effect of load-sharing on efficiency. The load power is shared by the battery (P_{Bat}) and generator (P_{Gen}) using a discrete load factor (α) as shown in (21) and (22), where i is the number of batteries ($i \epsilon [1, 2, 3]$) and j is the number of generators ($j \epsilon [1, 2, 3, 4, 5, 6]$), n and m are total number of operational batteries and generators, respectively.

$$P_{Bat,i} = \alpha \cdot \frac{P_{Total}}{n} \tag{21}$$

$$P_{Gen,j} = (1 - \alpha) \cdot \frac{P_{Total}}{m} \tag{22}$$

When α is 0, the total power demand is supplied only by the generator, whereas it is supplied only by the battery when α is 1. Based on the value of α ($\alpha \epsilon [0, 0.1, 0.2, \ldots, 0.9, 1.0]$), the load is shared between the batteries and the generators. The obtained energy efficiency for the fixed loads is presented in Fig. 6, which shows that the higher the usage of the battery, the higher the efficiency. Moreover, for the lower fixed load, the fuel consumption in the diesel generator increases, as shown by the SFOC curve in Fig. 5. Therefore, efficiency in the lower load condition is less compared to the higher load condition.

4.2. Efficiency analysis for real-case load profile and rule-based load-sharing

In the second case, the simulation is extended to a rael vessel profile and the operating time of almost 120 h for the complete power system as shown in Fig. 1. Here, again the case study is divided into two power system configuration scenarios which are common in marine operation, namely "common bus" and "sectionalized buses". These scenarios are formed based on the status of the bus-tie breakers that are located between the DC bus sections (see Fig. 1) such as closed bus-tie and open bus-tie, respectively. Here, they are referred to as scenario-1 and scenario-2. It also requires two different high-level control algorithms in the PEMS, as the way of operation of energy carriers varies from common bus to sectionalized buses.

In scenario-1, both bus-tie breakers are closed, shaping a common busbar for the whole vessel power system. The PEMS decides the number of operating engines based on the total load in the system. In this case, the batteries are designed to operate equally, meaning that all three batteries discharge or charge equally. In scenario-2, both bus-tie breakers are opened, resulting in three main individual buses. Each bus is then operating in an isolated mode. The load in each bus is supplied by the battery and generators connected in that bus. The results are given and compared for the two scenarios in the following figures.

The instantaneous efficiency due to the variation in the load profile and the power supplied by the diesel generators and the batteries is shown in Fig. 7(a). Further, the total energy efficiency variation during the simulation period for the common and sectionalized buses is shown in Fig. 7(b). Similarly, the total fuel consumption and corresponding CO_2 emissions using the battery as energy storage is presented in Fig. 7(c).

The average energy efficiency obtained during this operation is 46.7% and 48.8% for the common and sectionalized buses, respectively. However, the fuel consumptions and CO_2 emissions for both cases are similar. It indicates that the battery in the sectionalized bus supplies more energy compared to the one in the common bus. It is also shown by the final battery SoCs, which are 62.1% and 46.2%, respectively, for the common and sectionalized buses. The mentioned SoCs are the average of all batteries. Further, all the batteries were initialized at 60% SoC.

Further, the operational conditions are investigated based on the total running time and energy supplied to the bus, as shown in Fig. 8. The running time is expressed in the percentage of total simulation time, where energy carries supplied power to the bus. Therefore, for the batteries, the operational time when they are in discharging mode is only considered. Fig. 8(a) shows that the running time among the generators is uneven, where generator 1 is mainly operating, generator 2 is operating for almost 50% of the time, whereas generator 3 is briefly operating in the common bus. In contrast, generators are more evenly operational in the sectionalized buses. Therefore, it shows that the common bus has the potential to reduce the active number of generators connected to the bus. Furthermore, the batteries in the common bus are discharging for a longer duration than in the sectionalized buses.

Fig. 8(b) shows that generator 1 is the primary energy supplier in the common bus, whereas all three active generators supply evenly in the sectionalized bus. Further, batteries in the common bus supply less energy than the sectionalized buses. It is the main reason why the

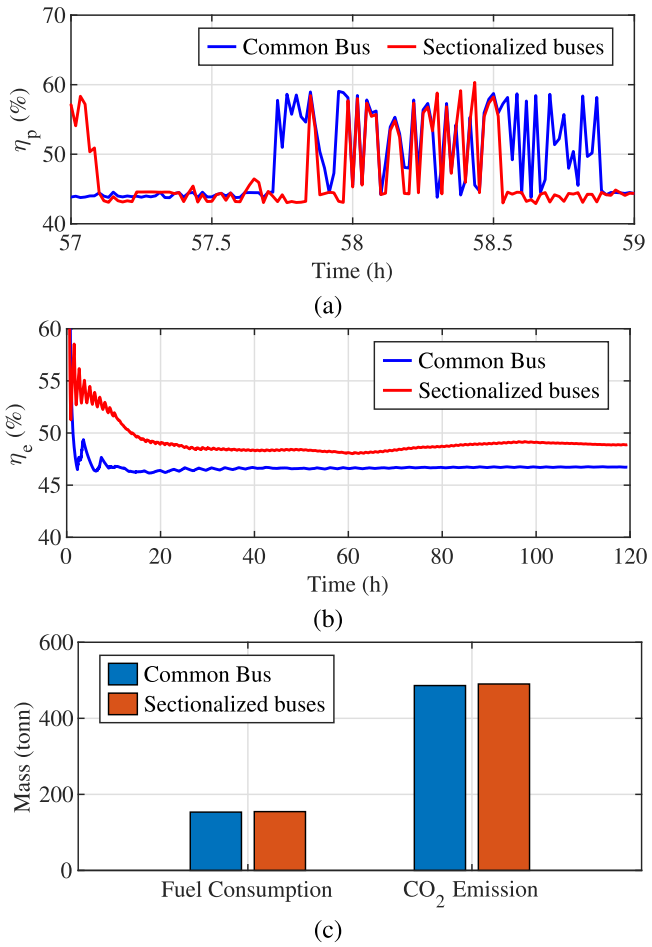

Fig. 7. Load profile-based efficiency and emissions analysis. (a) Power (instantaneous) efficiency variation. (b) The total energy efficiency variation against time. (c) The total accumulated fuel consumption and CO_2 emissions.

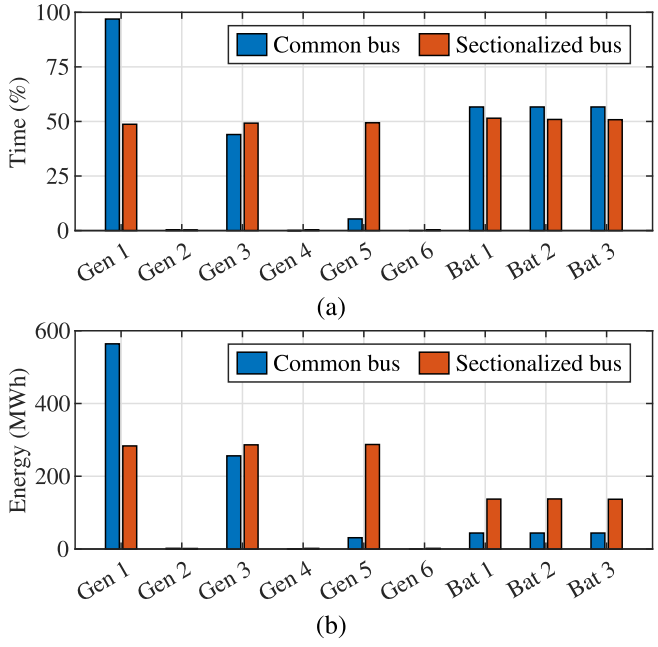

Fig. 8. Operational parameters of energy carries. (a) Running time in percentage. (b) Accumulated power (energy) output from the energy carriers to the bus.

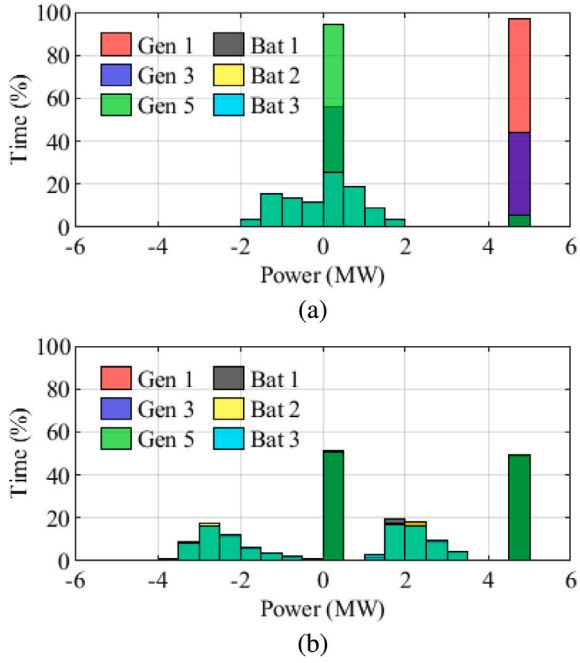

Fig. 9. Load distribution among the energy carriers. (a) Common bus. (b) Sectionalized bus.

energy efficiency during the operation with the sectionalized buses was higher than the common bus.

Although the batteries are operational for a longer duration in the common bus, they are not supplying as much energy as in the sectionalized bus. Therefore, to analyze the case, the load distribution among the energy carriers is performed and presented in Fig. 9. It shows that the batteries loading in the common bus are within 0 to 2 MW, whereas 0 to 3.5 MW in the sectionalized buses. It is due to the load-sharing strategies implemented in the PEMS, as the main principle in both cases is to operate a minimum number of diesel generators at the fuel-optimal region.

5. Conclusion

In this paper, an efficiency model has been developed for the marine hybrid power systems based on the physics- and data-based component models. The component models are integrated into a unified system model that can be applied to study the fuel efficiency of marine vessels. A semi-submersible drilling rig with all-electric propulsion and hybrid DC power system is used for the case studies. The simulation of the system model enabled the evaluation of the total fuel consumption, thereby CO_2 emissions from the vessel while supplying the vessel load demand. The energy efficiency and emissions are estimated in the sectionalized and common bus configurations on the studied vessel. Further, the total energy supplied by the generators and batteries along with their operational time and load distribution, are investigated. The results show that the energy efficiency in the sectionalized bus is slightly higher than the common bus for the studied vessel, which can be due to the load profile and the implemented load-sharing strategies in the PEMS. In addition, the sectionalized bus offers redundancy to the power system in case of worst-case failures. The proposed framework can further be used to evaluate and perform sensitivity analysis of the high-level control algorithms such as PEMS. This enables to design the future ship power and propulsion systems to comply with the environmental regulations.

CRediT authorship contribution statement

Pramod Ghimire: Writing – original draft, Writing – review & editing, Investigation, Methodology, Conceptualization. **Siamak Karimi:** Writing – original draft, Writing – review & editing, Methodology, Conceptualization. **Mehdi Zadeh:** Writing – review & editing, Supervision, Conceptualization. **Krishna Kumar Nagalingam:** Resources, Writing – review & editing. **Eilif Pedersen:** Writing – review & editing, Supervision, Conceptualization.

Declaration of competing interest

The authors declare that they have no known competing financial interests or personal relationships that could have appeared to influence the work reported in this paper.

Acknowledgment

This work was supported in part by the Research Council of Norway under Project 290455 and in part by Kongsberg Digital AS, Norway.

References

[1] P. Ghimire, D. Park, M. Zadeh, J. Thorstensen, E. Pedersen, Shipboard electric power conversion: System architecture, applications, control, and challenges [technology leaders], IEEE Electrif. Mag. 7 (4) (2019) 6–20, http://dx.doi.org/10.1109/MELE.2019.2943948.

[2] M.B. Othman, N.P. Reddy, P. Ghimire, M. Zadeh, A. Anvari-Moghaddam, J.M. Guerrero, A hybrid power system laboratory: Testing electric and hybrid propulsion, IEEE Electrif. Mag. 7 (4) (2019) 89–97, http://dx.doi.org/10.1109/MELE.2019.2943982.

[3] IMO, Fourth IMO GHG Study 2020 Full Report, Tech. Rep., International Maritime Organization, London, 2021, pp. 1–524.

[4] DNV, EEXI | Energy efficiency existing ship index - DNV, 2021, URL https://www.dnv.com/maritime/insights/topics/eexi.

[5] DNV, CII - Carbon intensity indicator - DNV, 2021, URL https://www.dnv.com/maritime/insights/topics/CII-carbon-intensity-indicator/index.html.

[6] J.B. Nielsen, Modeling and Simulation for Design Evaluation of Marine Machinery Systems (Ph.D. thesis), NTNU, Norwegian University of Science and Technology, Trondheim, 2019, pp. 22–27.

[7] B. Zahedi, L.E. Norum, K.B. Ludvigsen, Optimized efficiency of all-electric ships by dc hybrid power systems, J. Power Sources 255 (2014) 341–354, http://dx.doi.org/10.1016/j.jpowsour.2014.01.031.

[8] P. Ghimire, M. Zadeh, J. Thorstensen, E. Pedersen, Data-driven efficiency modeling and analysis of all-electric ship powertrain; a comparison of power system architectures, IEEE Trans. Transp. Electrif. (2021) 1, http://dx.doi.org/10.1109/TTE.2021.3123886.

[9] R. Prenc, A. Cuculić, I. Baumgartner, Advantages of using a DC power system on board ship, Pomor. Zb. 52 (1) (2016) 83–97, http://dx.doi.org/10.18048/2016.52.05.

[10] A.J. Sorensen, R. Skjetne, T. Bo, M.R. Miyazaki, T.A. Johansen, I.B. Utne, E. Pedersen, Toward safer, smarter, and greener ships: Using hybrid marine power plants, IEEE Electrif. Mag. 5 (3) (2017) 68–73, http://dx.doi.org/10.1109/mele.2017.2718861.

[11] C. Nuchturee, T. Li, H. Xia, Energy efficiency of integrated electric propulsion for ships – A review, Renew. Sustain. Energy Rev. 134 (2020) 110145, http://dx.doi.org/10.1016/j.rser.2020.110145.

[12] P. Ghimire, M. Zadeh, E. Pedersen, J. Thorstensen, Dynamic modeling, simulation, and testing of a marine DC hybrid power system, IEEE Trans. Transp. Electrif. 7 (2) (2021) 905–919, http://dx.doi.org/10.1109/TTE.2020.3023896.

[13] S. Karimi, M. Zadeh, J.A. Suul, Evaluation of energy transfer efficiency for shore-to-ship fast charging systems, in: 2020 IEEE 29th Int. Symp. Ind. Electron., IEEE, 2020, pp. 1271–1277, http://dx.doi.org/10.1109/ISIE45063.2020.9152219.

[14] A.K. Ådnanes, M. Oslo, B. Wolak, M. Houston, Design and control system status and inventions in electrical power and thruster systems for drillships and semi submersible rigs, in: Dyn. Position. Conf., 2004, pp. 1–15.

[15] C.-H. Kim, Y.-S. Kim, H.-W. Jung, S.-N. Ryu, K.-K. Yoon, Electric power system design and analysis for drilling rigs, J. Adv. Mar. Eng. Technol. 36 (7) (2012) 942–947, http://dx.doi.org/10.5916/JKOSME.2012.36.7.942.

[16] S. Lebedevas, L. Norkevičius, P. Zhou, Investigation of effect on environmental performance of using lng as fuel for engines in seaport tugboats, J. Mar. Sci. Eng. 9 (2) (2021) 1–19, http://dx.doi.org/10.3390/jmse9020123.

[17] E.K. Dedes, D.A. Hudson, S.R. Turnock, Assessing the potential of hybrid energy technology to reduce exhaust emissions from global shipping, Energy Policy 40 (1) (2012) 204–218, http://dx.doi.org/10.1016/j.enpol.2011.09.046.

[18] J.W. Kolar, H. Ertl, F.C. Zach, Influence of the modulation method on the conduction and switching losses of a PWM converter system, IEEE Trans. Ind. Appl. 27 (6) (1991) 1063–1075, http://dx.doi.org/10.1109/28.108456.

[19] A. Wintrich, U. Nicolai, W. Tursky, T. Reimann, Application Manual Power Semiconductors, Semikron International GmbH, 2015, p. 466, Semikron.

[20] J. Robinson, D. Jovcic, G. Joós, Analysis and design of an offshore wind farm using a MV DC grid, IEEE Trans. Power Deliv. 25 (4) (2010) 2164–2173, http://dx.doi.org/10.1109/TPWRD.2010.2053390.

[21] T.A. Nguyen, D.A. Copp, R.H. Byrne, B.R. Chalamala, Market evaluation of energy storage systems incorporating technology-specific nonlinear models, IEEE Trans. Power Syst. 34 (5) (2019) 3706–3715, http://dx.doi.org/10.1109/TPWRS.2019.2909764.

[22] O. Tremblay, L.-A. Dessaint, Experimental validation of a battery dynamic model for EV applications, World Electr. Veh. J. 2009, Vol. 3, Pages 289-298 3 (2) (2009) 289–298, http://dx.doi.org/10.3390/WEVJ3020289, URL https://www.mdpi.com/2032-6653/3/2/289.

[23] Wartsila Marine Solutions, Wartsila engine online configurator, 2021, URL https://www.wartsila.com/marine/engine-configurator.

[24] Infineon Technologies A.G., IGBT Modules - Infineon Technologies, URL https://www.infineon.com/cms/en/product/power/igbt/igbt-modules/.

[25] Vishay, Vishay Standard Recovery Diodes, (Hockey PUK Version), 3800 A, URL www.vishay.com.